

Shear-induced permeability changes in a polymer grafted silica membrane

Robert P. Castro¹, Harold G. Monbouquette, Yoram Cohen*

Department of Chemical Engineering, University of California, Los Angeles, CA 90095, USA

Received 14 February 2000; received in revised form 2 June 2000; accepted 20 June 2000

Abstract

The hydrodynamic response of a graft-polymerized membrane was demonstrated for a microporous silica-poly(vinylpyrrolidone) (silica-PVP) membrane. The membrane pores were modified by graft polymerizing vinyl pyrrolidone onto the membrane pore surface, resulting in a polymer surface layer of covalently tethered polymer chains. The hydraulic permeability of the modified membrane increased with increasing transmembrane pressure owing to flow-induced deformation of the grafted polymer chains. The dynamics of the modified pores was investigated by membrane hydraulic permeability studies along with a two-region hydrodynamic pore flow model. The thickness of the grafted polymer layer decreased with increasing pore-wall shear rate by up to about 47%, relative to the thickness at the zero shear limit, depending on the surface density and length of the grafted chains. Although the effective pore size of the polymer-grafted membrane was reduced by 5–36% (at the zero shear rate limit), about 18–59% of the pore size loss was regained at high pore-wall shear rates. Increasing the degree of shear-induced permeability change is feasible by increasing the ratio of the polymer chain length/pore size ratio as well as the surface density of the grafted polymer phase. The present results suggest that hydrodynamic pore size control could provide an additional useful degree of freedom in operating polymer-modified filtration membranes. © 2000 Elsevier Science B.V. All rights reserved.

Keywords: Shear-induced permeability change; Graft-polymerized membrane; Hydraulic permeability; Ceramic membrane

1. Introduction

In recent years, there has been a growing interest in the chemical surface modification of synthetic membranes with the goal of improving membrane stability and selectivity. Chemical modifications of both polymeric and ceramic membranes by polymer grafting and graft polymerization techniques have demonstrated improved fouling resistance of microfil-

tration (MF) and ultrafiltration (UF) membranes [1–4] and improved selectivity and stability of pervaporation membranes [5–7]. A particularly interesting and promising use of polymer modification of membranes has been the control of membrane permeability (or pore size) in response to environmental conditions such as temperature [8–12], pH and ionic strength [13–15] and solvent power for organic solvents [1,2]. Adsorbed polymers have also been shown to significantly affect membrane performance as a consequence of the adsorbed polymer response to solvent power [16–18].

It has also been known, in the polymer literature, that adsorbed and grafted polymers may undergo deformation, depending on chain size and surface

* Corresponding author. Fax: +1-310-206-4107.

E-mail addresses: yoram@ucla.edu, yoram@seas.ucla.edu (Y. Cohen).

¹ Present address: World Minerals, 2500 Miguelito, Lompoc, CA 93436, USA.

Nomenclature

a	monomer size (Å)
c	empirical constant, Eq. (7)
D	grafted chain spacing (Å)
D_e	hydrodynamic pore diameter (Å)
h	polymer brush height (Å)
J_{H_2O}	permeate water flux (cm/s)
K	Kozeny constant
K_o	pore shape factor
k	membrane hydraulic permeability (cm ²)
k_{CSP}	hydraulic permeability of CSP membrane (cm ²)
k_{H_2O}	hydraulic permeability (cm ²)
k_{un}	hydraulic permeability of unmodified support membrane (cm ²)
L	membrane thickness (cm)
L_e	equivalent pore length (cm)
N	average number of monomers per chain
ΔP	transmembrane pressure (g cm/s ² /cm ²)
R_{CSP}	hydrodynamic pore radius of polymer-modified membrane (Å)
R_e	effective hydrodynamic pore radius of unmodified support (Å)
R_i	inside tube radius (cm)
R_{MCSP}	resistance of polymer-modified membrane (m ⁻¹)
R_{Mun}	resistance of unmodified membrane (m ⁻¹)
R_o	outside tube radius (cm)
S_m	specific surface area (m ² /g)
$V^{(B)}$	interstitial velocity in brush region (cm/s)
$V^{(O)}$	interstitial velocity in outer (non-brush) region (cm/s)
\bar{V}_{CSP}	average interstitial velocity in polymer-modified membrane (cm/s)
V_o	superficial velocity (cm/s)
V_p	specific pore volume (m ³ /g)

Greek symbols

δ	effective hydrodynamic thickness of polymer brush layer (Å)
ϵ	porosity

ϕ_p	polymer volume fraction in polymer brush layer
γ_R	shear rate (s ⁻¹)
κ	Brinkman permeability coefficient (cm ²)
μ	fluid viscosity (g/cm/s)
σ	polymer graft density, Eq. (15)
τ	tortuosity

density, in response to hydrodynamic conditions. Early experimental studies, with high molecular weight polymers (typically $M_w > 10^5$), have demonstrated that polymers adsorbed onto pore walls of capillary tubes [18], channels [19,20], porous membranes [17,21] or packed beds [22,23] undergo flow-induced deformation. Investigations using analytical and numerical simulations [19,24–29] have also illustrated that terminally anchored chains are deformed in simple laminar shear flow. At sufficiently high shear rates, the polymer layer thickness decreases with increasing solvent shear rate, while the chains stretch in a direction parallel to the flow direction. Therefore, it is expected that, for polymer-modified MF and UF membranes, hydrodynamic conditions (i.e. pore-wall shear rate) could have a measurable impact on pore size when the permeate is also a good solvent for the polymer surface phase. This interplay between pore size and pore-wall shear rate, which has not been previously reported in the literature for membrane applications, is the subject of the present investigation.

The present study is a natural extension of recent studies on a new class of ceramic-supported polymer (CSP) membranes [1,2]. These membranes are formed by free-radical graft polymerization (FRGP) of a vinyl monomer onto the surface of porous silica supports previously activated by surface-grafting of vinyl silanes [30,31]. Using the above graft polymerization approach, we demonstrate the hydrodynamic pore size response of polyvinylpyrrolidone (PVP)-modified silica membranes.

2. Analysis

Modification of the membrane pore surface with a grafted polymer phase reduces the original pore size. Pore size reduction can be quantified in terms of the effective hydrodynamic thickness (EHT) of the

tethered polymer surface layer. The EHT is defined as the apparent thickness of an impermeable surface layer which would reduce the pore size to a level that accounts for the observed hydraulic permeability reduction. The EHT, δ , can be determined, using the capillary model for the pore structure, from the following relation [18,22,23,32]:

$$\frac{\delta}{R_e} = 1 - \left(\frac{k_{CSP}}{k_{un}} \right)^{0.25} = 1 - \left(\frac{R_{Mun}}{R_{MCSP}} \right)^{0.25} \quad (1)$$

in which k_{CSP} , R_{MCSP} and k_{un} , R_{Mun} are the hydraulic water permeabilities and membrane resistances (see Eq. (13)) of the modified and unmodified membranes, respectively. The unmodified effective hydrodynamic pore radius, R_e , is determined from [33]

$$R_e = \frac{D_e}{2} = \frac{2V_p}{S_m} \quad (2)$$

in which D_e is the effective pore diameter and V_p and S_m denote the pore volume and surface area per unit mass of the porous membrane, respectively. Finally, the modified pore radius R_{CSP} is given as

$$R_{CSP} = R_e - \delta \quad (3)$$

The grafted polymer chains can undergo shear-induced deformation, accompanied by tilting of the terminally anchored chains, in the flow direction, as the permeate flux increases (Fig. 1). As a result, the thickness of the grafted polymer brush layer will decrease with increasing shear rate in the pores. If the solvent penetrates the polymer brush layer, the polymer layer thickness can be estimated from a simple model that considers solvent permeation through the polymer brush layer. This model divides the flow field into two regions (Fig. 1): a fully developed flow region which consists of a brush layer that extends from the wall ($r = R_e$) to the edge of the polymer surface region ($r = R_e - h$, where h is the thickness of the polymer layer) and an outer region extending from the center of the pore ($r = 0$) to the edge of the brush layer (Fig. 1). The permeation rate through the brush (B) and outer (O) pore regions can be calculated from the predicted velocity profiles in each region. In the brush layer, the Debye–Brinkman equation can be used to describe permeation through the porous membrane [28,33,34]:

$$\frac{1}{r} \frac{d}{dr} \left(r \frac{dV^{(B)}}{dr} \right) - \frac{V^{(B)}}{\kappa} + \frac{dP}{dx} \frac{1}{\mu} = 0 \quad (4)$$

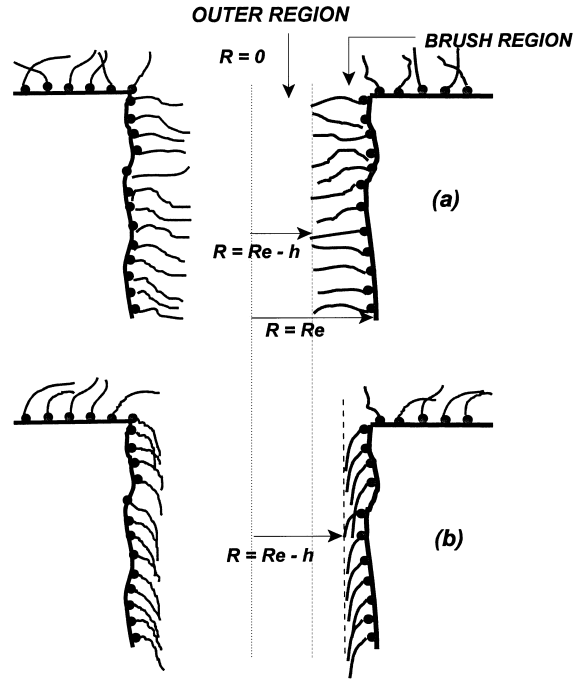


Fig. 1. Schematic illustration of a two-region pore model: (a) low shear rate (i.e. low permeate flow); (b) high shear rate (i.e. high permeate flow). Permeation into the pore is from top to bottom.

where $V^{(B)}$ is interstitial velocity in the brush layer, parallel to the pore wall, μ is the solvent viscosity, r is the radial distance from the pore center normal to the pore wall, dP/dx is the pressure gradient along the pore path and κ is the solvent-specific hydraulic permeability coefficient of the brush layer.

In the outer region, the equation of motion in the axial direction reduces to

$$\frac{1}{r} \frac{d}{dr} \left(r \frac{dV^{(O)}}{dr} \right) + \frac{dP}{dx} \frac{1}{\mu} = 0 \quad (5)$$

where $V^{(O)}$ is the interstitial velocity in the outer region. Eqs. (4) and (5) are solved simultaneously to obtain the coupled flow in the porous region and the core of the tube, subject to the boundary conditions

$$V^{(B)} = 0 \quad \text{at } r = R_e \quad (6a)$$

$$\frac{dV^{(O)}}{dr} = 0 \quad \text{at } r = 0 \quad (6b)$$

$$\frac{dV^{(B)}}{dr} = \frac{dV^{(O)}}{dr} \quad \text{at } r = R_e - h = h^* \quad (6c)$$

$$V^{(B)} = V^{(O)} \quad \text{at } r = R_e - h = h^* \quad (6d)$$

in which h is the height of the brush layer and where Eqs. (6c) and (6d) represent the continuity of stress (or velocity gradient when the fluid viscosity is shear-independent) and velocity at the brush layer/outer region boundary. Values of the permeability coefficient (κ) of the brush layer, which are required to obtain a solution to Eq. (4), can be estimated from the following empirical correlation [34]:

$$\kappa = c \left(\frac{1 - \phi_p}{\phi_p} \right) \quad (7)$$

where ϕ_p is the polymer volume fraction in the polymer layer and c is an empirical constant determined from polymer sedimentation data for each polymer/solvent system. Using experimental sedimentation coefficient data for the PVP/water system [35,36], which is the focus of the present study, the solvent

permeability in the polymer phase was evaluated, as a function of polymer volume fraction (Fig. 2) with a value $c = 5.54 \times 10^{-15} \text{ cm}^2$. In reality, the polymer volume fraction, ϕ_p , will vary with position across the polymer surface layer. In the present analysis, however, ϕ_p is approximated to be uniform across the thin tethered polymer surface layer. Therefore, consistent with the simple scaling model of de Gennes [37], the polymer volume fraction in the surface polymer layer is estimated as

$$\phi_p = \frac{Na\sigma}{h} \quad (8)$$

in which h is the polymer layer thickness, N is the number of monomers per grafted chain, a is the monomer size and σ is the polymer graft density (i.e. $\sigma = (a/D)^2$; where D is the distance between polymer anchoring points on the surface).

Given the predicted velocity profiles for a model pore, the permeate flux through the modified membrane is calculated for a specified polymer layer thickness by integrating the composite interstitial velocity

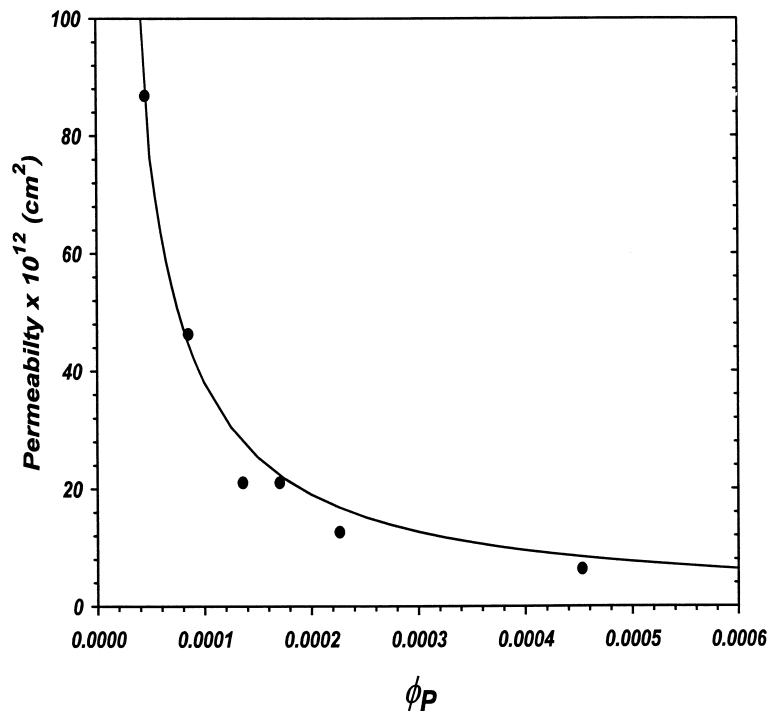


Fig. 2. Variation of water permeability with polymer volume fraction for PVP. (Data source: [35,36].)

profile:

$$\bar{V}_{\text{CSP}} = \left(\frac{2\pi}{\pi R_e^2} \right) \left[\int_0^{h^*} rV^{(O)}(r) dr + \int_{h^*}^{R_e} rV^{(B)}(r) dr \right] \quad (9)$$

where $h^* = R_e - h$. The superficial velocity (i.e. permeate flux) at the shell-side of the membrane tube, V_o , is related to the average interstitial (pore) velocity [38]:

$$V_o = \frac{\bar{V}_{\text{CSP}}\epsilon}{\tau} \quad (10)$$

in which τ is the tortuosity of the membrane that can be calculated as $\tau = (K/K_o)^{0.5}$, where K is the Carmen–Kozeny constant (Eq. (14)) and $K_o = 2$ for a capillary pore geometry [38]. The tortuosity is also often expressed as the ratio L_e/L [38], where L_e is the effective fluid path in the porous matrix, and thus, the Carmen–Kozeny constant is given — $K = K_o(L_e/L)^2$.

At a given transmembrane pressure, the polymer layer thickness can be estimated by matching the calculated water permeate flux from Eq. (10) with the measured value. The procedure involves the numerical solution of Eqs. (4) and (5) followed by the evaluation of Eqs. (9) and (10), for a given value of h which is selected by an iterative procedure to converge to the experimental flux. The calculated polymer layer thickness was correlated with the unmodified pore-wall shear rate, $\dot{\gamma}_R$, defined as [23,39]

$$\dot{\gamma}_R = \frac{8\bar{V}_{\text{CSP}}}{D_e} \quad (11)$$

where \bar{V}_{CSP} is the average interstitial pore velocity (Eq. (9)).

3. Experimental

3.1. Materials

Isotropic porous silica tubular supports (MicroPorous Glass) with a pore size of 2000 Å were obtained from the Asahi Glass Company (Tokyo, Japan). The

Table 1
Physical properties of unmodified silica tubular membrane supports

	Tube I	Tube II	Disc B ^a
Pore size ^b (Å)	2000	2000	1200
Hydraulic diameter (Å)	3210	3210	1550
Thickness (cm)	0.1	0.1	0.0519
Inside diameter (cm)	0.8	0.8	
Length (cm)	21	21	
Weight (g)	6.386	5.975	1.079
Surface area (m ²)	42.2 ^c	39.4 ^c	13.8 ^d
Pore volume (cm ³)	3.38 ^e	3.17 ^e	0.39 ^f
Porosity	0.48	0.45	0.43
$k_{\text{H}_2\text{O}}^g$ (cm ²)	8.84×10^{-12}	8.84×10^{-12}	1.73×10^{-12}
Kozeny constant (K)	3.49	3.27	3.76

^a [2].

^b Nominal pore size provided by manufacturer.

^c Specific surface area = 6.60 m²/g.

^d Specific surface area = 9.27 m²/g.

^e Specific pore volume = 0.53 cm³/g (provided by manufacturer).

^f Specific pore volume = 0.36 cm³/g (provided by manufacturer).

^g Hydraulic water permeability.

physical properties of the supports, including the surface area, as determined by BET analysis (Autosorb-1, Quantachrome Inc., Buffalo, NY), are given in Table 1.

Vinyltrimethoxysilane (H₂C=CH-Si-(OCH₃)₃) and hydrogen peroxide (30 vol.% aqueous solution) were obtained from Aldrich (Milwaukee, WI). Xylenes (ACS grade), 1-vinyl-2-pyrrolidinone monomer and potassium hydroxide were obtained from Fisher Scientific (Pittsburg, PA), and ammonium hydroxide (58 vol.% aqueous solution) was obtained from Mallinckroft Inc. (Paris, KY).

3.2. Surface modification

3.2.1. Overview

The CSP membranes were prepared by FRGP of vinyl pyrrolidone chains onto the surface of the given support material, resulting in terminally and covalently-bonded PVP chains [30,31,40]. Modification of the membrane supports followed the general methodology of Jou et al. [5], adapted for vinylpyrrolidone graft polymerization. Surface modification of the support membrane was performed in three sequential steps: (a) pretreatment; (b) surface activation and (c) graft polymerization.

3.2.2. Pretreatment

The silica substrate was first treated with a 2% aqueous HCl solution to clean the substrate and to fully hydrate the surface. The membranes were subsequently rinsed and dried with the membrane weight followed gravimetrically until the desired moisture level was reached. The subsequent silylation step involved the modification of –OH groups, present on the ceramic pore surface, by chemical grafting of VTMS to generate vinyl surface sites for the subsequent surface polymerization reaction. A fully hydroxylated silica surface has a hydroxyl concentration of about 4.6 –OH groups/nm² [41]. Correspondingly, monolayer layer coverage by vinylsilane would yield a maximum of about 7.6 μmol vinyl silane/m² silica surface. Surface water, however, is known to allow for a higher silylation coverage via the formation of a polysilane network which is covalently anchored to the silica surface [42–44]. Therefore, the initial density of surface vinyl sites, and thus, the resulting polymer surface chain density can be controlled, in part, by surface moisture content.

3.2.3. Surface silylation

Silylation of tubular porous membrane supports was performed by circulating a 10% (v/v) vinyltrimethoxysilane (VTMS)/xylenes solution from a reaction flask, fitted with a condenser, through the tube-side of the support with a diaphragm pump (Model 7090-42, Cole Palmer Co., Chicago, IL); the permeate stream was recycled to the feed reservoir. The reaction was carried out at the boiling point of xylene (137°C) over a period of 5 h with the condenser temperature set above the boiling point of methanol (70°C) in order to remove the methanol by-product from the reaction mixture. The flow through the tube-side of the support was kept at the laminar flow regime ($N_{Re} \leq 1460$) to maintain tangential flow at the membrane surface. The transmembrane pressure was adjusted using a needle valve, located at the tube-side outflow, so as to maintain permeate flow through the porous support.

The hydrophilicity of the silylated surface decreased due to the grafting of VTMS. However, since graft polymerization with PVP was performed in an aqueous solution, it was necessary to restore the hydrophilicity of the surface by hydrolyzing the unreacted alkoxy groups. Hydrolysis was accomplished by immersing the silylated membrane supports in potas-

sium hydroxide/water solution (pH = 9.5) for 3 days (with stirring). The modified membrane supports were then rinsed with distilled water until neutral pH was achieved.

3.2.4. Surface graft polymerization

PVP chains were grown from vinyl surface sites using *N*-vinyl-2-pyrrolidone as a monomer in an aqueous solution. Graft polymerization of the silylated tubular membrane supports was conducted in situ in a cross-flow operation. The reaction mixture was recirculated (from a 1 l reaction vessel) through the membrane module at a tube-side Reynolds number (in the membrane tube-side) of about 1500; this provided a residence time of approximately 16 s in the reaction loop. Mixing of the reaction mixture was promoted by constant stirring of the content of the reactor vessel. All reactions were carried out at 70°C for a period of 8 h with a nitrogen blanket in the reaction vessel. Nitrogen atmosphere was necessary to eliminate atmospheric oxygen, which is known to increase the latent period of polymerization and reduce the rate of polymerization. The grafting reaction was initiated with the addition of 1 ml of hydrogen peroxide solution (30 vol.% in H₂O) and 0.4 ml of ammonium hydroxide solution (58%) to the reaction vessel. Ammonium hydroxide acts as a buffer for the reaction mixture and prevents the formation of the undesirable acetaldehyde byproduct under acidic conditions. In addition, ammonium hydroxide has a strong activating effect on the polymerization reaction, shortening the latent period and increasing the rate of reaction. At the termination of the reaction, the PVP-modified membrane was rinsed by flowing distilled water tangentially, followed by dead-end filtration flow mode to remove unattached PVP chains from the membrane matrix.

Two different tubular membrane supports were grafted using a 0.938 M monomer solution (Tube I-A) and a 2.81 M solution (Tube II). At the termination of the permeability experiments with Tube I-A, this membrane was subjected to a second graft polymerization treatment with the 0.938 M monomer solution. The second sequential grafting added to the polymer graft yield due to additional grafting onto previously unreacted surface vinyl groups (Table 2). In addition to the tubular membranes, a porous disk filter, previously characterized by Castro et al. [2] and modified with PVP, at a higher surface chain density than for

Table 2
Surface properties of silylated and graft-polymerized silica-PVP membranes

Membrane	Silane coverage ($\mu\text{mol}/\text{m}^2$)	Graft yield (mg/m^2)	Chain density ($\mu\text{mol}/\text{m}^2$)	Chain spacing (\AA)	σ^a	\bar{M}_n^b (g/mol)	N^c	$N^{-6/5}$
Tube I-A	12.9	0.137	0.0458	60.2	0.0113	3000	27	0.0192
Tube I-B	12.9	0.277	0.0924	42.4	0.0228	3000	27	0.0192
Tube II	10.9	1.70	0.0596	52.8	0.0147	28500	257	0.00128
Disc B	20.2	2.06	0.11	38.8	0.0272	18600	168	0.00214

^a σ : polymer graft density.

^b Number-average molecular weight.

^c Average number of monomer units per chain.

the tubular membranes (Table 2), was utilized to assess the behavior of a high surface density PVP layer. The silylation coverage and polymer graft yields for the modified membranes were determined gravimetrically as previously described by Castro et al. [1,2].

Direct observation of the topology of the grafted PVP chains in the membrane was not feasible since that required imaging of a relatively rough surface, in addition to sacrificing the membrane. Instead, a PVP-modified silicon (100) prime-grade silicon wafer (Wafernet, San Jose) of root-mean-square surface roughness of 0.2 nm was utilized for atomic force microscopy (AFM) imaging of the PVP surface layer. The wafer was first soaked in acetone followed by methanol. The wafer was then immersed in a 7:3 (by volume) solution of sulfuric acid (certified ACS grade, Fisher Scientific) and 30% hydrogen peroxide in water. The wafers were dried under vacuum at 110°C and subsequently silylated and graft polymerized under the same reaction conditions as for the polymer membranes. AFM imaging was performed using a Digital Instrument multimode atomic force microscope with a Nanoscope IIIa SPM controller, operating in the tapping mode.

3.3. Permeability measurements

Hydraulic permeability measurements with the unmodified and modified tubular supports were conducted at 23°C in a cross-flow configuration with the apparatus shown in Fig. 3. The tubular membrane support was set in a stainless steel module housing (1T1-70 Sanitary Module, US Filter, Warrendale, PA). Water was pumped through the tubular membrane using either a peristaltic (Cole Palmer, Chicago, IL) or diaphragm (Model A304010210, Flojet Corp., Irvine,

CA) pump. Feed flow rate was monitored with an in-line flowmeter (Model F-45376LHN-8, Blue White Industries, Westminster, CA). Pressure monitoring at the inlet (P_1) and outlet (P_2) of the membrane module, relative to atmospheric pressure, was accomplished using pressure transducers (Model CD223, Validyne Engineering Company, Northridge, CA). The transmembrane pressure, computed based on the average of P_1 and P_2 , was adjusted by manipulating the retentate line needle valve (Model NV40025T, Hayward Industrial Products, Elizabeth, NJ).

The hydraulic permeability of the modified and native tubular membranes, $k_{\text{H}_2\text{O}}$ was determined from Darcy's law:

$$k_{\text{H}_2\text{O}} = \frac{J_{\text{H}_2\text{O}} \mu_{\text{H}_2\text{O}} R_o \ln(R_o/R_i)}{\Delta P_m} \quad (12)$$

with the membrane resistance, R_m , defined as

$$R_m = \frac{R_o \ln(R_o/R_i)}{k_{\text{H}_2\text{O}}} \quad (13)$$

where $J_{\text{H}_2\text{O}}$ is the measured water permeate flux (at the membrane shell-side), $\mu_{\text{H}_2\text{O}}$ is the water viscosity, ΔP_m is the transmembrane pressure, and R_o and R_i are the outside and inside membrane tube radii, respectively. We note that the membrane permeability, $k_{\text{H}_2\text{O}}$, for the native (i.e. unmodified) membrane support, can be related to the effective pore diameter [33]:

$$k_{\text{H}_2\text{O}} = \frac{\epsilon D_e^2}{16K} \quad (14)$$

where K is the Carmen–Kozeny constant determined for a specific membrane support from hydraulic permeability measurements, given D_e as calculated from Eq. (2).

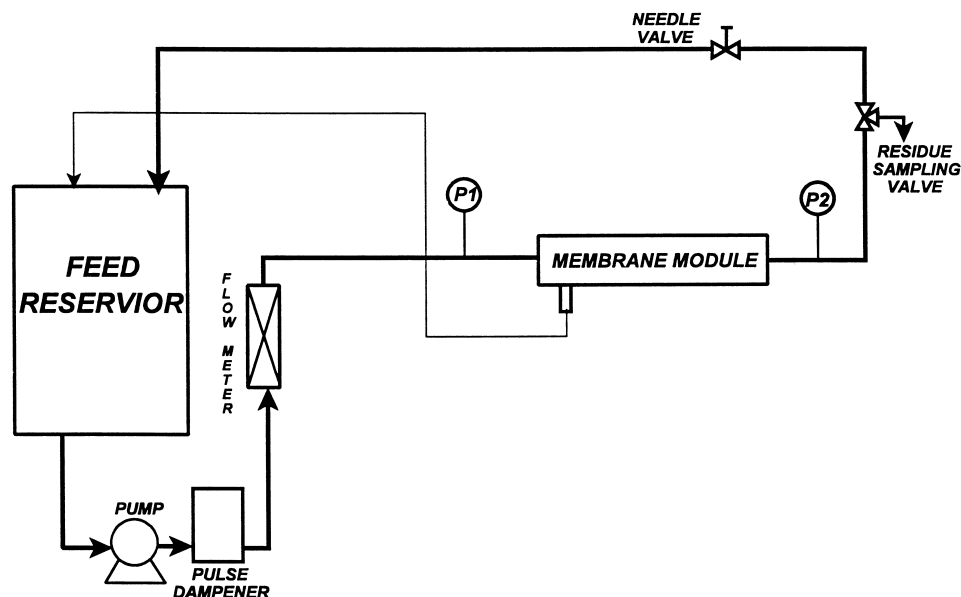


Fig. 3. Cross-flow filtration apparatus for tubular supports and modified membranes.

4. Results and discussion

4.1. Surface modification

The unmodified ceramic membrane supports were characterized by hydraulic permeability measurements with the membrane characteristics listed in Table 1. For the range of Kozeny constants (3.27–3.76), calculated for the present membranes, the tortuosity (see Eq. (10)) ranges from 1.28 to 1.37. These values are slightly lower than for unconsolidated porous matrices but within the expected range. For example, for a single sphere, the effective path, relative to the sphere diameter is $\pi/2$ which is equivalent to a tortuosity of about 1.57 and the value for L_e/L of about $\sqrt{25/12}$ is often cited in the literature for unconsolidated packed beds of spheres [38].

The ceramic membranes were silylated and subsequently modified with PVP with the corresponding silylation coverage and polymer graft yield given in Table 2. The surface-modified silica membranes resulted in PVP grafted chains of 27–168 monomers per chain and an average spacing of about 39–60 Å between chain anchoring points. We note that Tube I-B was formed by a second graft polymerization of Tube I-A. This resulted in the formation of new PVP

chains, initiated from previously unreacted surface vinyl silanes, and thus, additional increase in the polymer graft yield. For comparison, Tables 1 and 2 also include results for a previously reported silica disc support [1].

The surface density of the PVP surface chains is an important factor affecting the resulting conformation of the grafted chains. At sufficiently high surface densities, when the distance between chains is less than their radius of gyration, the grafted polymer chains extend away from the surface, to minimize their free energy, in a conformation analogous to the bristles of a brush. The grafted polymer layer is said to be in the so-called brush regime when the following criterion is satisfied [37]:

$$\sigma = \left(\frac{a}{D}\right)^2 > N^{-6/5} \quad (15)$$

where σ is the polymer graft density, N is the average number of monomer units per chain and a is the size of a monomer unit. The monomer size for PVP was determined to be 6.4 Å based on molecular calculations using the Spartan molecular modeling program (Spartan ver. 4.1, WaveFunction Inc., Irvine, CA). Comparison of polymer graft density (σ) and $N^{-6/5}$ (see Table 2) reveals that the grafted layers for Tube II and Disk B

were in the brush regime. In contrast, the grafted chains for Tube I-A were sparsely distributed on the surface; however, upon sequential grafting (Tube I-B), the polymer layer was in the dense regime.

We note, however, that both Tubes I-A and I-B had significantly shorter grafted polymer chains (Table 2).

The example AFM image of a graft-polymerized PVP surface shown in Fig. 4 is consistent with the

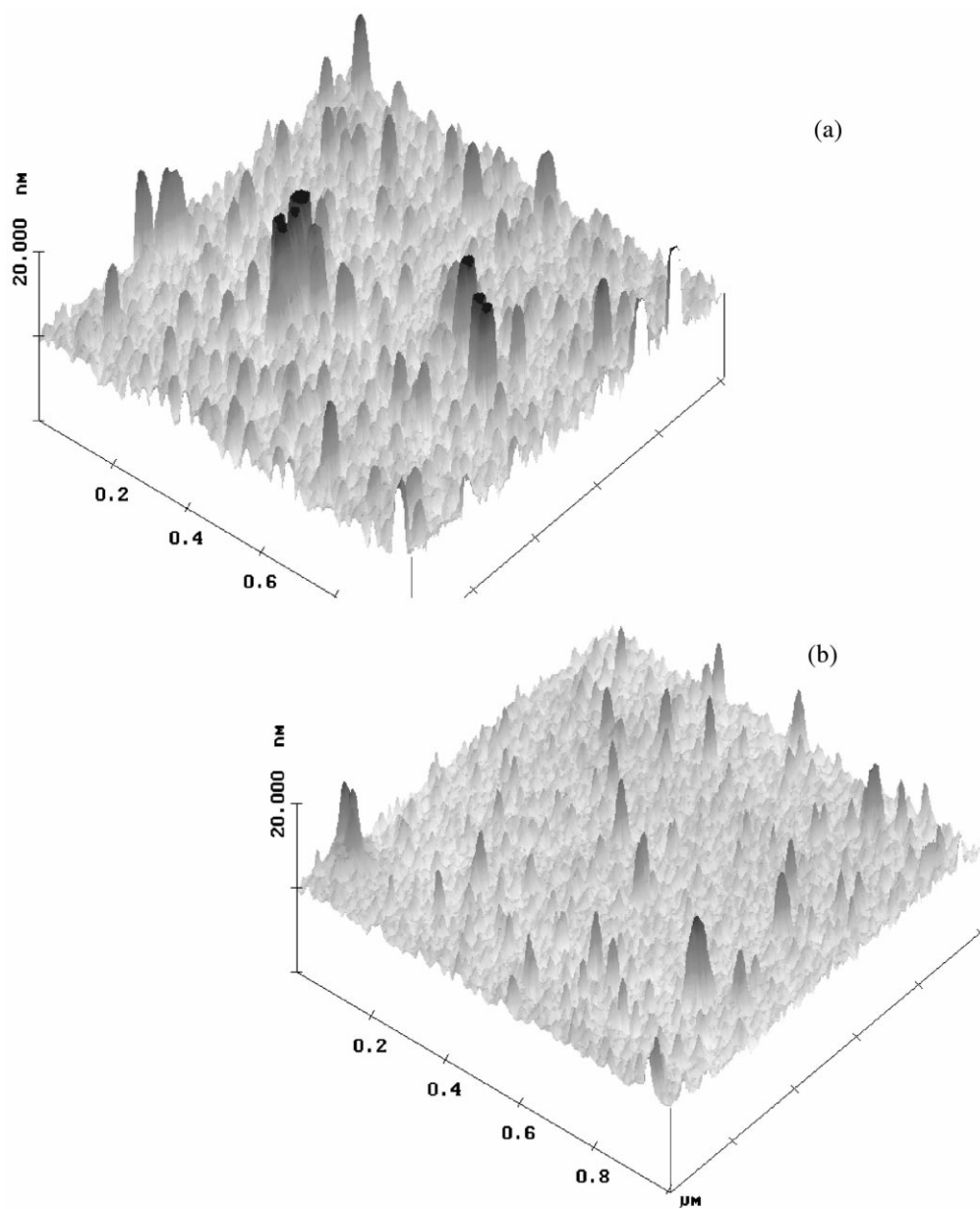


Fig. 4. AFM images of PVP grafted onto the surface of a silicon wafer by polymerization at 70°C with an initial monomer concentration of (a) 0.938 M and (b) 2.81 M.

expected polydispersed polymer layer for free-radical polymerization [31]. Surface topology indicates layer features that rise in excess of 20 nm which is consistent with the hydrodynamic thickness of the grafted layer discussed in Section 4.2. The root-mean-square surface roughness for the depicted graft-polymerized PVP surfaces, prepared with initial monomer concentrations of 0.938 and 2.81 M, were determined to be about 2.8 and 0.8 nm, respectively. The above results are supported by previous kinetic studies [30,31,40] in which it was shown that a rougher grafted PVP surface is expected for surfaces prepared with a lower initial monomer concentration for which grafting of growing chain from the bulk solution can be significant [40]. It is important to note that the AFM images were acquired under dry conditions, and thus, do not reflect the actual conformation of the surface layer when exposed to the solvent. Nonetheless, the images clearly demonstrate that the surface is fully covered with PVP chains, with regions between the larger chains (or collection of large chains) populated with shorter PVP chains.

4.2. Hydraulic permeability and brush hydrodynamics

The modification of the porous membranes with tethered PVP chains resulted in membrane resistance (or permeability) behavior (Fig. 5) which depends on

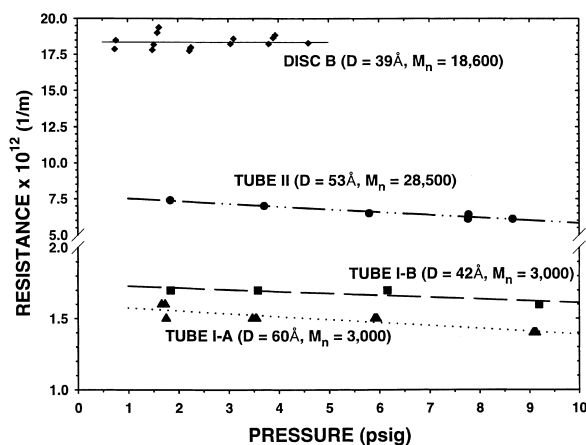


Fig. 5. Variation of membrane resistance with transmembrane pressure for modified silica-PVP membranes. (D = chain spacing, M_n = number-average molecular weight of grafted chains.)

the characteristics of the polymer surface layer (Table 2). The decrease in membrane resistance (or increase in permeability), for the range of transmembrane pressure studied, for the tubular membranes (I-A, I-B and II) suggests a pore diameter which increases with increasing permeate flow. The above behavior has been documented in the literature for laminar solvent shear flow past adsorbed and grafted polymers [18,19,28,29]. Under quiescent conditions, the terminally anchored chains are at their maximum extension away from the pore surface. Therefore, at low permeate flow rates (or at low pore-wall shear rates), pore size reduction is at its highest. As permeate flow (or pore-wall shear rate) increases with increasing transmembrane pressure, the polymer chains are stretched and tilted in the flow directions, resulting in an apparent pore diameter increase. The above behavior supports the prospect of developing a membrane in which the polymer layer can be utilized to impart a degree of hydrodynamic pore size control. Such a hydrodynamic response could add another dimension to proposed ‘chemical valve’ membranes that are actuated by changes in pH, temperature and solvent quality [13–15,45].

Disk B, which had a denser surface chain density relative to Membrane Tubes I and II (Table 2), exhibited an essentially constant membrane resistance which was also higher than those of the tubular membranes. Apparently, the polymer surface density was sufficiently high, such that the polymer layer did not deform and its thickness was thus invariant with pore-wall shear rate for the range investigated in this study. We note that shear-independent behavior of tethered polymers was previously reported in the study of Webber et al. [21] for toluene flow over a shear rate range 10^3 – 10^4 s^{-1} , for a ‘dense’ brush layer ($\sigma \approx 0.01$ – 0.02) of tethered polystyrene ($M_w = 45,000$ – $185,500$), formed by adsorption of poly(2-vinylpyridine)/polystyrene di-block copolymer onto a porous mica support.

The thickness of the polymer surface layer, under permeate flow conditions, was quantified in terms of both the EHT and the two-region model thickness (TRMT) as described in Section 2. The results shown in Figs. 6 and 7 reveal that the EHT is lower than the TRMT by about 7–54%, over the experimental ranges of polymer graft yields and shear rates. This is not surprising since the two-region model accounts

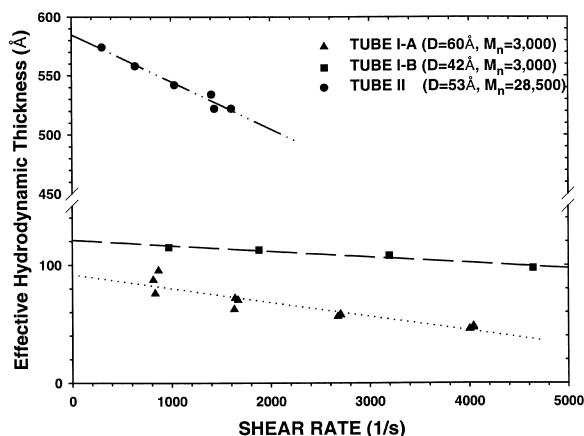


Fig. 6. Shear rate dependence of the effective hydrodynamic thickness (EHT) for PVP-grafted membranes. (D = chain spacing, M_n = number-average molecular weight of grafted chains.)

for solvent flow through the polymer surface layer. Permeability loss is therefore due to solvent/polymer interaction over a greater region of the pore space. On the other hand, the EHT model assumes a compact and impermeable configuration for the polymer phase, and thus, yields a lower polymer layer thickness. The variation of both the EHT and TRMT with pore-wall shear rate follows the membrane resistance dependence on shear rate. For Membrane Disk B, the EHT and the TRMT were independent of shear rate (therefore not shown in Figs. 6 and 7), with average

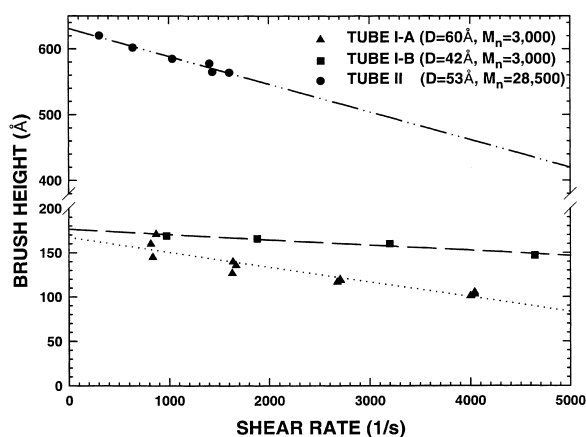


Fig. 7. Shear-rate dependence of the grafted PVP layer height determined from the two-region model.

values of 283 and 320 Å, respectively. It is noted that maximum pore size reduction is expected at the zero shear rate limit (see Figs. 6 and 7) where the chains achieve their maximum vertical extension (i.e. away from the pore surface). In this extrapolated zero shear rate limit, pore size reduction for Tubes I-A, I-B and II and Disc B, relative to the unmodified membranes, was about 5.5, 7.5, 36 and 37%, respectively, based on the pore size reduction as determined by the EHT values.

It is convenient to compare the hydrodynamic behavior of the different membranes over the shear rate range extending from the extrapolated zero shear rate limit to the highest experimental shear rate (extrapolated as necessary, to the maximum shear rate of 4640 s^{-1} achieved with Tube I-B). Over the above shear rate range, the TRMT for Tubes II, I-A and I-B decreased by about 31, 47 and 15%, respectively, relative to the extrapolated zero shear-rate condition (Fig. 7); this corresponds to an increase in the effective pore size (relative to the zero shear rate limit) of 18, 3.5 and 1.5%, respectively, for the above three membranes. We note, however, that the polymer layer thickness for Disc B, for which the chain density was highest ($\sigma = 0.027$) was found to be independent of shear rate. Lack of shear response of grafted PVP was also reported in a previous work [46] in which it was shown that the permeability of size exclusion chromatography (SEC) columns, packed with PVP-grafted SEC silica resins, was independent of shear rate for a polymer surface graft density of $\sigma \approx 0.04$. Clearly, in order to design a membrane with a pore size which responds to hydrodynamic conditions, the polymer chain density cannot be so high as to prevent flow-induced deformation of the polymer phase.

Inspection of the velocity profiles in the modified membrane pores provides additional insight as to the role of the polymer surface layer (Fig. 8). The velocity profiles illustrated in Fig. 8 for modified Tube II ($\Delta P = 1.8$ and 8.7 psig) and Disc B ($\Delta P = 4.6$ psig), are displaced away from the pore wall with a nearly Darcy's plug-flow profile through a significant portion of the polymer layer. For Disc B, 7% of the total permeate flow occurred through the brush region. For Tube II, permeate flow through the polymer layer ranged from 2.9 to 2.2% for the pressure range 1.8–8.7 psig. In contrast, for Tubes I-A and I-B, the percentage of the permeate flow through the less dense

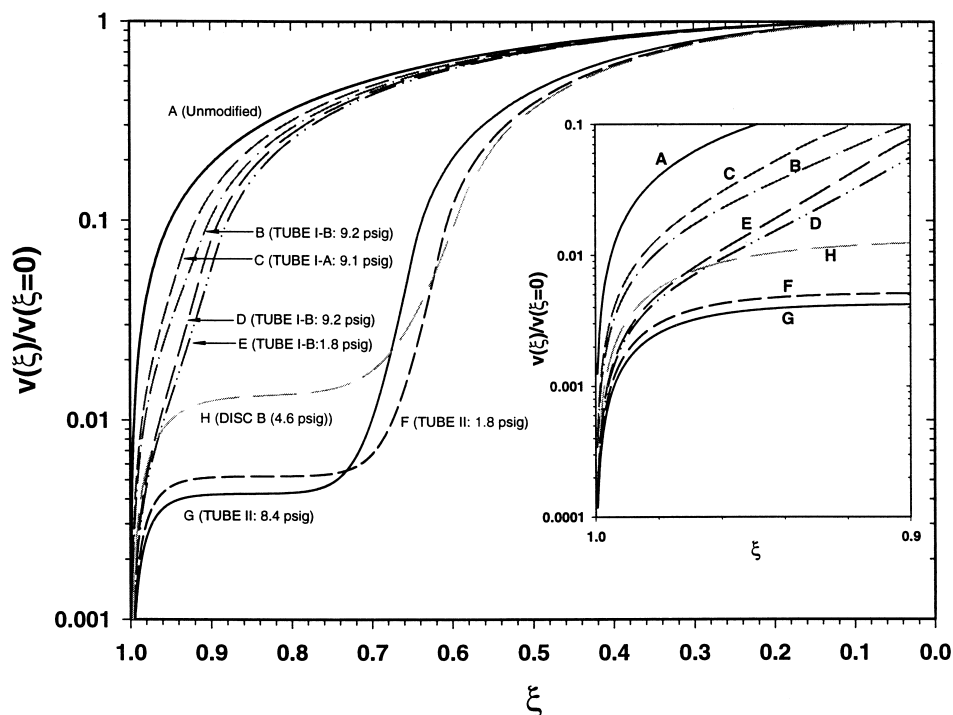


Fig. 8. Velocity profiles in unmodified (curve A) and PVP-modified membrane pores ($\xi = r/R_e$; pore center is at $\xi = 0$).

polymer layer of shorter chains was $<1\%$ for the same range of transmembrane pressure indicated in Fig. 8. It is also noted that the displacement of the velocity profiles from the pore wall for Tubes I-A and I-B is negligible, but the reduction in the local velocity, relative to the unmodified pore, was significant (Fig. 8). Tube II and Disc B had significantly longer grafted chains than Tube I (A and B), and thus, exhibited a greater displacement of the velocity profile from the pore wall. The behavior in Fig. 8 demonstrates that the impact of the grafted polymer layer is most pronounced for long and dense surface coverage. Clearly, a spectrum of chain behavior is expected, depending on the chain size and surface density.

Although the terminally grafted polymer chains reduce the membrane pore size, relative to the unmodified membrane, reduction in the polymer layer thickness with increasing shear rate resulted by about 18–59% regain of the pore size (i.e. diameter) loss at high shear rates. It is expected that, through optimal design of the polymer surface layer (i.e. chain size and surface density), improved tuning of the membrane

hydrodynamic pore size (or hydraulic permeability) could be feasible for practical applications.

5. Conclusions

The hydrodynamic alteration of membrane pore size was demonstrated for a new class of CSP membranes. The terminally anchored polymer layer should enable the synthesis of a membrane pore with a tethered polymer layer capable of altering the pore dimension in response to flow conditions. The effective membrane pore size decreases upon polymer grafting but increases with increasing transmembrane pressure. This behavior is attributed to flow-induced deformation of the grafted polymer phase. Flow-induced deformation should be measurable provided that: (a) the polymer surface layer in the pores consists of terminally anchored chains of sufficient length and surface density; and (b) the permeate solution is a good solvent for the polymer chains. With careful optimization of the grafted polymer phase, it is

envisioned that a hydrodynamically controlled pore size membrane could provide an additional useful degree of freedom in operating filtration membranes.

Acknowledgements

This work was supported in part by the US Department of Energy and the UC Universitywide Energy Research Group. A UCLA Pollution Prevention Fellowship to Robert Castro is also acknowledged. Wayne H. Yoshida prepared the modified wafers and obtained the AFM images at the DOE/William R. Wiley Environmental Molecular Sciences Laboratory in Richland, WA.

References

- [1] R.P. Castro, H.G. Monbouquette, Y. Cohen, The permeability behavior of polyvinylpyrrolidone-modified porous silica membrane, *J. Membr. Sci.* 84 (1993) 151.
- [2] R.P. Castro, Y. Cohen, H.G. Monbouquette, Silica-supported polyvinylpyrrolidone filtration membranes, *J. Membr. Sci.* 115 (1996) 179.
- [3] M. Ulbricht, G. Belfort, Surface modification of ultrafiltration membranes by low temperature plasma. II. Graft polymerization onto polyacrylonitrile and polysulfone, *J. Membr. Sci.* 111 (1996) 193.
- [4] H. Chen, G. Belfort, Surface modification of poly(ether sulfone) ultrafiltration membranes by low-temperature plasma-induced graft polymerization, *J. Appl. Polym. Sci.* 72 (1999) 1699.
- [5] D.-J. Jou, W. Yoshida, Y. Cohen, Pervaporation with ceramic-supported polymer membranes, *J. Membr. Sci.* 162 (1999) 269.
- [6] T. Yamaguchi, S. Yamahara, S. Nakao, S. Kimura, Preparation of pervaporation membranes for removal of dissolved organics from water by plasma-graft filling polymerization, *J. Membr. Sci.* 95 (1994) 39.
- [7] T. Yamaguchi, Y. Miyazaki, S. Nakao, T. Tsuru, S. Kimura, Membrane design for pervaporation or vapor permeation separation using a filling-type membrane concept, *Ind. Eng. Chem. Res.* 37 (1) (1998) 177.
- [8] H. Iwata, M. Odate, Y. Uyama, H. Memiya, Y. Ikada, Preparation of temperature-sensitive membranes by graft polymerization onto porous membranes, *J. Membr. Sci.* 55 (1991) 119.
- [9] S.-W. Chun, J.-D. Kim, A novel hydrogel-dispersed composite membrane of poly(*N*-isopropylacrylamide) in a gelatin matrix and its thermally actuated permeation of 4-acetaminophen, *J. Control Release* 38 (1996) 39.
- [10] Y. Okahata, H. Noguchi, T. Seki, Thermoselective permeation from a polymer-grafted capsule membrane, *Macromolecules* 19 (1986) 493.
- [11] T. Tomoya, M. Konno, S. Saito, Permeation mechanism for a thermo-sensitive composite membrane composed of porous glass and *n*-isopropylacrylamide, *J. Chem. Eng. Jpn.* 23 (1990) 447.
- [12] T. Tsuji, M. Konno, S. Saito, Permeation mechanism for a thermo-sensitive composite membrane composed of porous glass and *n*-isopropylacrylamide, *J. Chem. Eng. Jpn.* 23 (1990) 447.
- [13] K. Kontturi, S. Mafé, J.A. Manzanares, B.L. Svarfvar, P. Viinikka, Modeling of the salt and pH effects on the permeability of grafted porous membranes, *Macromolecules* 29 (1996) 5740.
- [14] Y. Ito, Y. Ochiai, Y.S. Park, Y. Imanishi, pH-sensitive gating by conformational change of a polypeptide brush grafted onto a porous polymer membrane, *J. Am. Chem. Soc.* 119 (1997) 1619.
- [15] M.A. Mika, R.F. Childs, J.M. Dickson, Chemical valves based on poly(4-vinylpyridine)-filled microporous membrane, *J. Membr. Sci.* 153 (1999) 45.
- [16] J.T. Kim, J.L. Anderson, Hindered transport through micropores with adsorbed polyelectrolytes, *J. Membr. Sci.* 42 (1989) 109.
- [17] W.K. Idol, J.L. Anderson, Effects of adsorbed polyelectrolytes on convective flow and diffusion in porous membranes, *J. Membr. Sci.* 28 (1986) 269.
- [18] Y. Cohen, The hydrodynamic thickness of adsorbed polymers in steady shear flow, *Macromolecules* 21 (1988) 494.
- [19] J.-J. Lee, G.G. Fuller, *Macromolecules* 17 (1984) 375.
- [20] I. Soga, G. Granick, Flow-induced deformation and desorption of adsorbed polymers, *Langmuir* 14 (1998) 4266.
- [21] R.M. Webber, J.L. Anderson, M.S. Jhon, Hydrodynamic studies of adsorbed diblock copolymers in porous membranes, *Macromolecules* 23 (1990) 1026.
- [22] P. Gramain, P. Myard, Elongational deformation by shear flow of flexible polymers adsorbed in porous media, *Macromolecules* 14 (1981) 180.
- [23] Y. Cohen, R. Christ, Hydrodynamic adsorption of macromolecules in porous media, *J. Reservoir Eng. SPE* (1986) 113–118.
- [24] A. Hatano, *Polymer* 25 (1984) 1198.
- [25] J.L. Anderson, P.F. Mackenzie, R.M. Webber, Model for hydrodynamic thickness of thin polymer layers at solid/liquid interfaces, *Langmuir* 7 (1991) 162.
- [26] J.D. Atkinson, C.J. Goh, N. Phan-Thien, *J. Chem. Phys.* 80 (1984) 6305.
- [27] R.S. Parnas, Y. Cohen, The response of a terminally anchored polymer chain to simple shear flows, *Macromolecules* 24 (1991) 4646.
- [28] R.S. Parnas, Y. Cohen, A terminally anchored polymer chain in laminar shear flow: hydrodynamic interactions, *Rheol. Acta* 33 (1994) 485.
- [29] S.P. Doyle, E.S.G. Shaqfeh, A.P. Gast, Rheology of polymer brushes, *Macromolecules* 31 (1998) 5474.
- [30] M. Chaimberg, Y. Cohen, Free-radical graft polymerization of vinyl pyrrolidone onto silica, *Ind. Eng. Chem. Res.* 30 (1991) 2534.
- [31] M. Chaimberg, Y. Cohen, The kinetics of graft polymerization onto silica substrates, *AIChE J.* 40 (1994) 294.

- [32] R. Varoqui, P. Dejardin, Hydrodynamic thickness of adsorbed polymers, *J. Chem. Phys.* 66 (1977) 4395.
- [33] F.A.L. Dullien, *Porous Media: Fluid Transport and Pore Structure*, Academic Press, New York, 1992.
- [34] M.A. Cohen Stuart, F.H.W.H. Waajen, T. Cosgrove, B. Vincent, T.L. Crowley, Hydrodynamic thickness of adsorbed polymer layers, *Macromolecules* 17 (1984) 1825.
- [35] L.E. Miller, F.A. Hamm, Macromolecular properties of polyvinylpyrrolidone: molecular weight distribution, *J. Phys. Chem.* 57 (1953) 110.
- [36] W. Scholtan, Molekulargewichtsbestimmung von Polyvinylpyrrolidon mittels der Ultrazentrifuge, *Makromol. Chem.* 7 (1953) 209.
- [37] P.G. DeGennes, Conformation of polymers attached to an interface, *Macromolecules* 13 (1980) 1069.
- [38] Y. Cohen, A.B. Metzner, Wall effects in laminar flow of fluids through packed beds, *AIChE J.* 27 (1981) 75.
- [39] Y. Cohen, C. Chen-Nian, The flow of microemulsions through packed beds and capillary tubes, *Chem. Eng. Commun.* 28 (1984) 73.
- [40] Y. Cohen, R. Faibish, M. Rovira, Size exclusion chromatography with graft polymerized silica resins, in: E. Pfefferkorn (Ed.), *Surface Interactions in Size Exclusion Chromatography*, Marcel Dekker, New York, 1999.
- [41] R.K. Iler, *The Chemistry of Silica*, Wiley, New York, 1979.
- [42] M. Chaimberg, Y. Cohen, Silylation of inorganic oxide supports, *J. Colloid Interface Sci.* 134 (1990) 576.
- [43] K.M.R. Kallury, P.M. MacDonald, M. Thompson, Effect of surface water and base catalysis on the silanization of silica by (aminopropyl)alkoxysilanes studied by X-ray photoelectron spectroscopy and ^{13}C cross-polarization/magic angle spinning nuclear magnetic resonance, *Langmuir* 10 (1994) 492.
- [44] G.S. Caravajal, D.E. Leydon, G.R. Quinting, G.E. Maciel, Structural characterization of 3-(aminopropyl)-triethoxysilane-modified silicas by ^{29}Si and ^{13}C nuclear magnetic resonance, *Anal. Chem.* 60 (1988) 1776.
- [45] S. Åkerman, P. Viinikka, B. Svarfvar, K. Putkonen, K. Järvinen, K. Kontturi, J. Näsman, A. Urttia, P. Paronena, Drug permeation through a temperature-sensitive poly(*N*-isopropylacrylamide) grafted poly(vinylidene fluoride) membrane, *Int. J. Pharm.* 164 (1998) 29.
- [46] Y. Cohen, P. Eisenberg, M. Chaimberg, Permeability of graft polymerized polyvinylpyrrolidone-silica resin in packed columns, *J. Colloid Interface Sci.* 21 (1992) 579.